Electrochemistry Communications 82 (2017) 47–51

Contents lists available at ScienceDirect

Electrochemistry Communications

journal homepage: www.elsevier.com/locate/elecom

Visible-light-promoted gas-phase water splitting using porous $WO_3/BiVO_4$ photoanodes

T. Stoll[a,1], G. Zafeiropoulos[a,1], I. Dogan[a], H. Genuit[a], R. Lavrijsen[b], B. Koopmans[b], M.N. Tsampas[a,*]

[a] DIFFER-Dutch Institute For Fundamental Energy Research, De Zaale 20, 5612 AJ Eindhoven, The Netherlands
[b] Department of Applied Physics, Eindhoven University of Technology, 5600 MB Eindhoven, The Netherlands

ARTICLE INFO

Keywords:
Photoelectrochemical H_2 production
Polymeric electrolyte membrane
Gas phase water-splitting
$WO_3/BiVO_4$ photoanode
Visible light

ABSTRACT

We recently described the use of Ti(0) microfibers as an anodization substrate for the preparation of TiO_2 nanotubes arrays as porous photoanodes. Here, we report the use of these fibers as a scaffold to build porous photoanodes based on a $WO_3/BiVO_4$ heterojunction. The obtained photoelectrodes show promising results under visible light irradiation for water oxidation both in a typical liquid-phase photoelectrochemical setup and in a gas phase reactor (developed in-house) based on a polymeric electrolyte membrane.

1. Introduction

With the rise of energy and climate concerns, a large number of research teams around the world are working on the development of devices to produce hydrogen from water and solar energy. In the ideal case, these photoelectrochemical (PEC) devices or cells would make possible, under light irradiation, the dissociation of water into its fundamental components, hydrogen and oxygen. In this context, the use of semiconductor-based water-splitting systems is a promising route towards production of “solar hydrogen” at an affordable price [1,2].

The main challenges in the field are the development of efficient photoelectrodes and scalable reactor design [1–3]. This work focuses on the development of a PEC design which resembles polymeric electrolytic membrane (PEM) electrolysers and is thus called PEM-PEC [3]. This type of reactor has the advantage of being compact, robust and easily scalable. However it requires a porous photoelectrode rather than the planar design built on conducting glass substrates used in conventional PEC studies. Up to now only simple photoanodes based on TiO_2 or WO_3 have been developed for PEM-PEC applications [4–6]. These materials can absorb only a small fraction of the solar terrestrial illumination and as a result their performance is very limited [4–6]. In order to adapt the PEM-PEC concept to the visible part of the solar spectrum, the scope of this article is to investigate the possibility of using the well-known heterojunction $WO_3/BiVO_4$ [2,7].

$BiVO_4$ in its scheelite type monoclinic phase possesses promising properties for applications as a photoanode in photoelectrochemical cells. With an ~2.4 eV band gap, it can, in theory, under 1 sun illumination produce photocurrents up to 7 $mA{\cdot}cm^{-2}$ for the water splitting reaction at the thermodynamic potential [1,2]. However, in practice, this material is susceptible to fast hole/electron pair recombination leading to a significant performance drop [7–9]. Some solutions have been tested to overcome this issue: the addition of a doping metal (e.g. W, Mo) [8,9] to diminish the recombination or the association with another semiconductor through the formation of a heterojunction (i.e. $WO_3/BiVO_4$) to enhance the charge separation [7]. WO_3 is a semiconductor with an indirect band-gap around 2.8 eV that provides light absorption in the near UV and at the beginning of the visible spectrum [1] and has recently been reported to be compatible with titanium microfibers as electric back contact [10]. Due to its good charge carrier properties and to the band alignment with the bands of $BiVO_4$, the electrons from the $BiVO_4$ conduction band can be injected into WO_3, enhancing the charge separation and thus the efficiency [1,2,7].

In this study we built $WO_3/BiVO_4$ heterojunctions on porous titanium substrates by combining electrochemical anodization of sputtered tungsten layers and $BiVO_4$ formation via the SILAR (Successive Ionic Layer Adsorption and Reaction) [11] method, and successfully used them to perform gas phase water-splitting. Although most of the common methods (i.e. spin-coating, doctor blade, hydrothermal synthesis) [2] cannot be used in this case, the aforementioned preparation techniques suit the nature and the specific porous morphology of the electrode substrate particularly well.

* Corresponding author.
E-mail address: m.tsampas@differ.nl (M.N. Tsampas).
[1] First and second authors contributed equally and possess the 1st authorship of the article.

http://dx.doi.org/10.1016/j.elecom.2017.07.019
Received 7 June 2017; Received in revised form 21 July 2017; Accepted 25 July 2017
Available online 27 July 2017

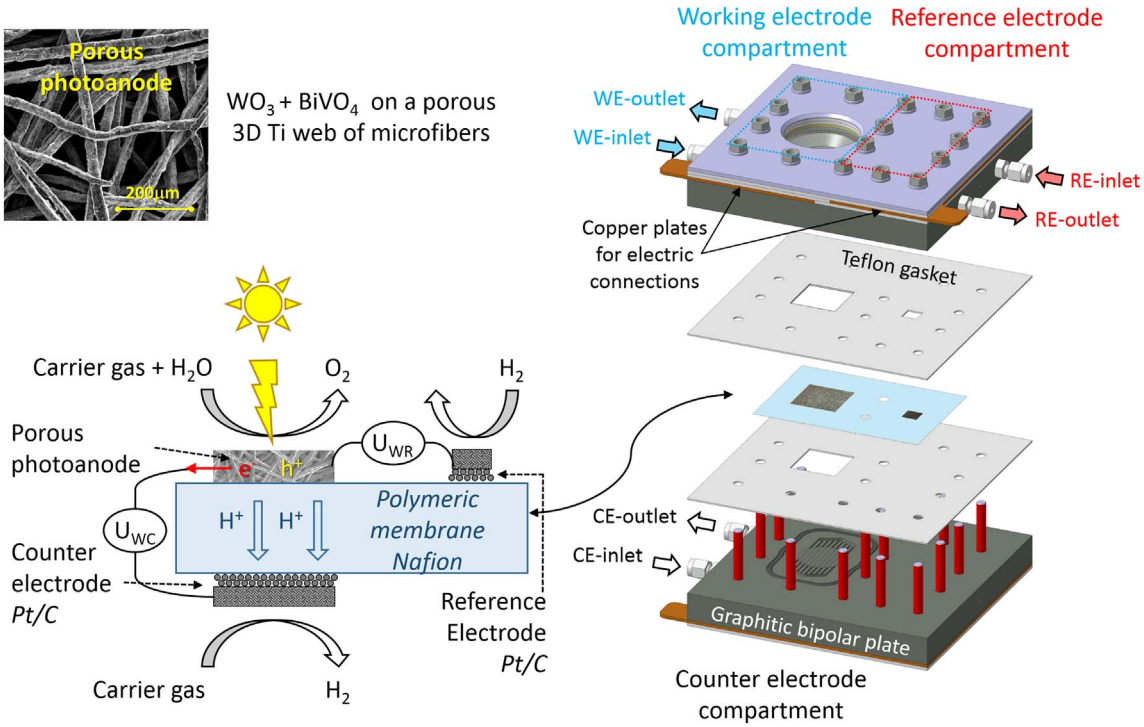

Fig. 1. (Left) Configuration and operation of the membrane (photo)electrode assembly. (Right) Novel PEM-PEC reactor design with three compartments for accommodating photoanode, cathode and reference electrodes [3].

2. Experimental

W thin films were deposited by DC magnetron sputtering (Kurt J. Lesker) from a 2 in. metallic W target (Kurt J. Lesker) on Ti substrates (Bekaert) of 0.3 mm thickness, 80% porosity, 20 µm microfibers and 99.9% purity [3]. W-deposition was carried out with base pressure ~ 10^{-8} mbar, a target–substrate distance of 95 mm at 25 °C, under Ar pressure of 1 Pa, and a power of 100 W. The resulting W-film thickness was 200 nm. WO_3 layers were formed through anodization of the 200 nm layer of W(0). To form the oxide a potential of 30 V was applied for 2 min in an ethylene glycol solution containing 0.3 wt% NH_4F and 2 vol% H_2O. Then the electrode was rinsed with water prior to a calcination step (500 °C for 1 h). One SILAR cycle for the $BiVO_4$ deposition is described as follows: the electrode is dipped for 1 min in a 0.05 M $BiNO_3$ solution, dried for 1 min, rinsed in miliQ-water for 30 s, dried for 30 s, dipped in 0.05 M ammonium metavanadate (NH_4VO_3) (pH = 2) solution for 1 min, dried for 1 min, rinsed in miliQ water for 30 s and dried for 30 s. Once the desired number of cycles has been reached the samples are calcined at 550 °C for 1 h and then etched for 20 min in 1 M KOH solution to remove the unwanted vanadium binary oxide (V_2O_5) [12]. The amount of deposited $BiVO_4$ is therefore controlled by the number of cycles performed.

Surface morphologies of the photoanodes were characterized using a scanning electron microscope (FEI Quanta 3D FEG instrument) at an acceleration voltage of 30 keV and a working distance of 10 mm. The crystal phases were analyzed by X-ray diffraction (Brucker D8 Advance Eco) using a Cu K_α tube. Diffuse reflectance spectra were obtained using a UV–Vis spectrophotometer (PerkinElmer-Lamda 1050) with an integrating sphere attachment (150 mm InGaAs). A Hiden QGA quadrupole mass spectrometer (M/S) operating in selected ion mode with a SEM detector was used for the detection of oxygen and hydrogen in the anodic and cathodic gas streams. Raman spectroscopy measurements were performed with a Renishaw Raman microscope equipped with a 514 nm laser, a grating with 1800 lines/mm, and a CCD detector, and with a measurement step size of 1.7 cm^{-1}. The laser power during measurements is fixed at 0.3 $W{\cdot}mm^{-2}$.

The photoelectrodes (geometrical area ca. 1 cm^2) were illuminated using a 150 W Xe lamp (66477-150XF-R1, Newport) with a UV cut-off filter (< 395 nm) and an IR removal water filter, where the light intensity was adjusted with a reference cell and meter certified by Newport (91150V) to 100 $mW{\cdot}cm^{-2}$ on the photoelectrode surface. The lamp in both cases was positioned at the same distance (3 cm) from the photoelectrode surface and the illumination density was measured in both conventional and PEM-PEC reactors to ensure that the power was the same. The dark current and photo-current of the working electrode versus the external bias voltage were recorded using an Ivium-CompactStat potentiostat, at a 10 $mV{\cdot}s^{-1}$ scan-rate. Liquid phase photoelectrochemical water-splitting experiments were performed at pH = 1 (0.1 M H_2SO_4) in a conventional PEC cell while gas phase experiments were carried out in our novel PEM-PEC cell (Fig. 1) both are described in detail in a previous paper [3]. Each compartment of the PEM-PEC was fed with gaseous streams, made by bubbling He or air for anodic, He for cathodic and H_2 for reference compartment (at 50 $ml{\cdot}min^{-1}$) through thermostatted gas saturators (at 25 °C) containing H_2O, leading to 3.5 vol% H_2O in the feeds.

3. Results and discussion

3.1. Structural analysis

Five samples were characterized: pure Ti/TiO_2 substrate (Ti_{web}), and substrates covered with W(0), WO_3, $BiVO_4$ and WO_3/$BiVO_4$. Fig. 2A shows the XRD patterns of the different samples. Typical diffraction peaks from the titanium substrate (black line) are clearly observed for all the samples, along with some smaller signals that can be attributed to a thin over-layer of rutile TiO_2 [3]. In the XRD pattern of the W(0) sputtered sample (blue line) three new signals can be seen at 44, 58 and 74° in good agreement with literature [2,4]. Those peaks are still present after the anodization plus annealing processes (green line), suggesting the formation of a thin WO_3 layer since none of its typical peaks are detected.

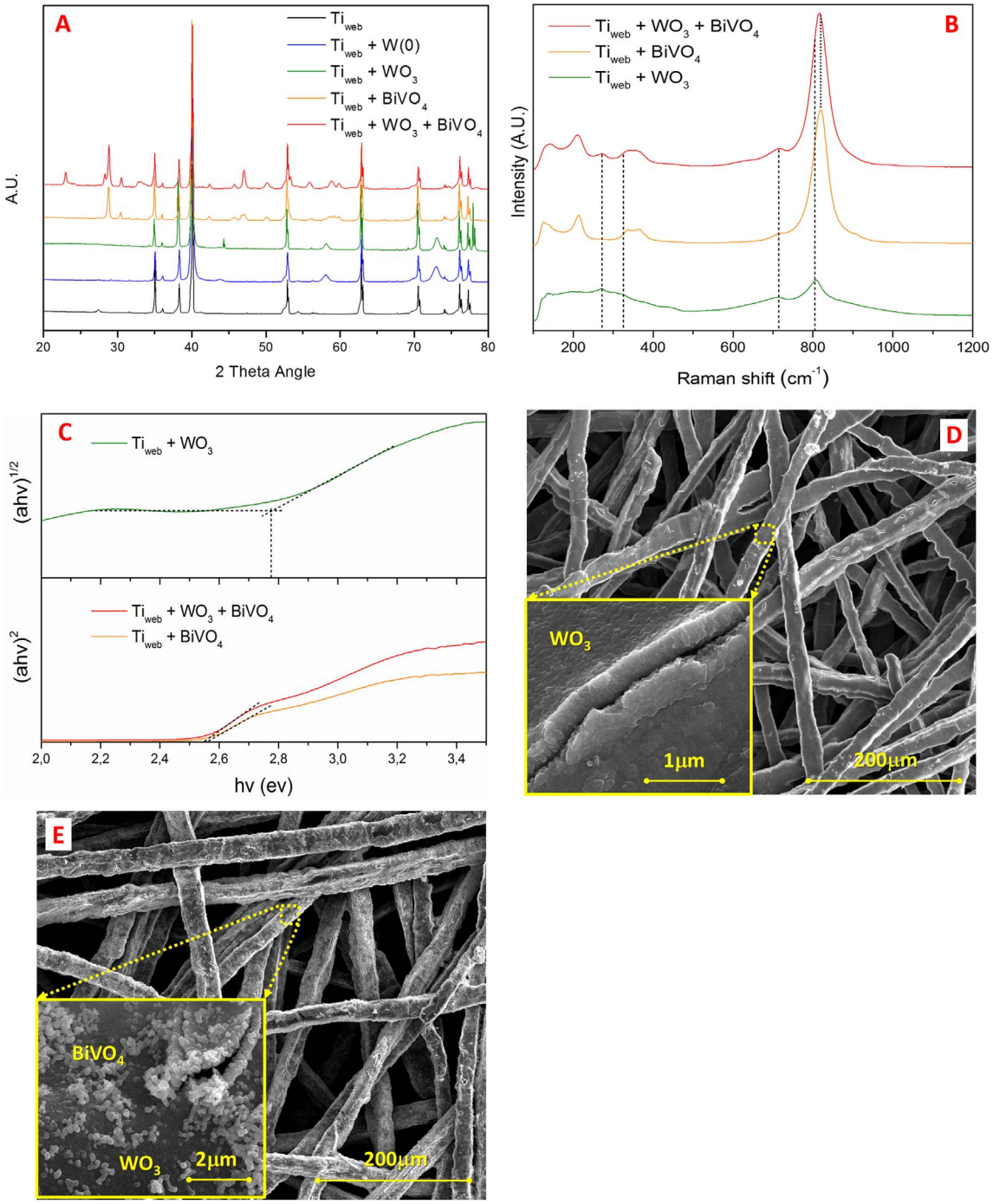

Fig. 2. (A) XRD diffraction patterns of the original Ti_{web} and with different added layers. (B) Raman spectra of Ti_{web}-based photoanodes covered by WO_3, $BiVO_4$ and $WO_3/BiVO_4$. (C) Tauc plot of the photoanodes for band gap determination. SEM images of Ti_{web} covered by (D) WO_3 and (E) $WO_3/BiVO_4$. $BiVO_4$ and $WO_3/BiVO_4$ have a loading of 40 SILAR-cycles. (For interpretation of the references to color in this figure, the reader is referred to the web version of this article.)

Analysis of the $Ti_{web}/BiVO_4$ sample (orange line) shows typical peaks for a monoclinic scheelite structure at angle values of 19, 29, 35, 40, 42, 45, 47, 53, and 58 [2,4], in addition to the substrate signals. These signals are still visible on the complete multilayered sample XRD pattern (red line) confirming the success of the $BiVO_4$ deposition process onto the WO_3. Since consecutive annealing steps were carried out for the fabrication of the $WO_3/BiVO_4$, the crystallinity of the WO_3 under-layer has changed compared to the Ti_{web}/WO_3 sample (green line). Thus, additional peaks at 24 and 29° are observed in the spectrum of the $Ti_{web}/BiVO_4$ sample (orange line), which are attributed to WO_3 [4].

As additional characterization we have performed Raman spectroscopy on the prepared photoanodes. This technique allows monitoring the local structure of the material and its bonding states near the surface. Therefore, we expect information mainly from the deposited WO_3 and/or $BiVO_4$ layers. Fig. 2B depicts the Raman spectra of WO_3 (green), $BiVO_4$ (orange) and $WO_3/BiVO_4$ (red) deposited on Ti_{web}. For the WO_3 structures, four main peaks are located at 272, 326, 717 and 807 cm^{-1} in good agreement with literature [13]. The $BiVO_4$ spectrum has six characteristic peaks located at 129, 213, 326, 366, 718 and 827 cm^{-1} [14]. It is clearly seen that the mixed structure $WO_3/BiVO_4$ has features both from WO_3 and $BiVO_4$ structures. The peak located at 815 cm^{-1} is

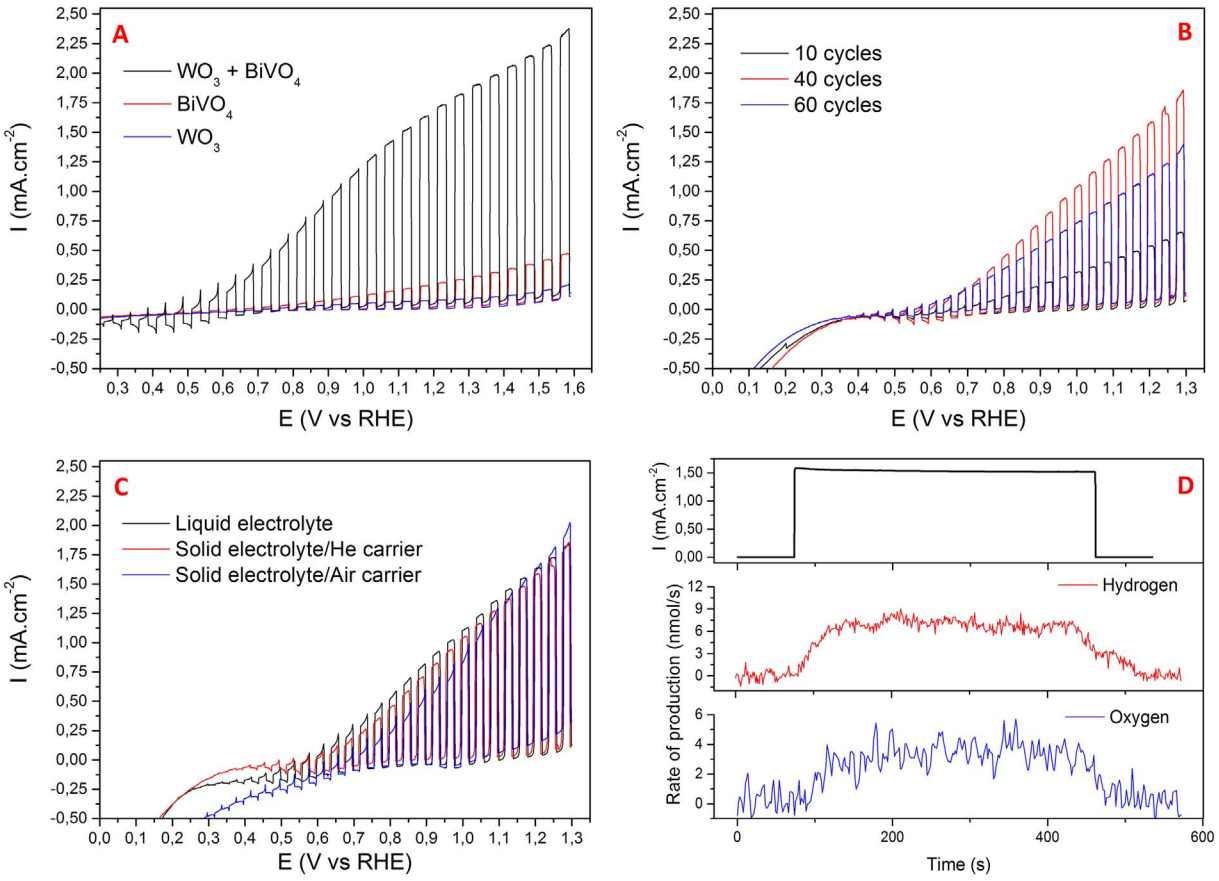

Fig. 3. Linear voltammetry sweeps (10 mV/s) of various photoanodes under chopped illumination for water splitting. (A) Independent $BiVO_4$ and WO_3 and their coupled conterpart (at 40 SILAR-cycles), (B) activity of $WO_3/BiVO_4$ photoanodes for different $BiVO_4$ loading, (C) 40 SILAR-cycles $WO_3/BiVO_4$ liquid vs gas phase activity (3.5 vol% H_2O in He or air). (D) Detection of oxygen and hydrogen generation during a step transient illumination experiment for $WO_3/BiVO_4$ (40 SILAR-cycles) at 1.23 V vs RHE.

a combination of the stretching mode of WO_3 located at 805 cm^{-1} and the stretching mode of $BiVO_4$ located at 827 cm^{-1}.

The optical band gap of our photoanodes was determined by the following Tauc equation: $(ah\nu)^n = A(h\nu - Eg)$ where A = constant, $h\nu$ = light energy, Eg = optical band gap energy, a = measured absorption coefficient, n = 0.5 for indirect band gap, and n = 2 for direct band gap materials [13]. WO_3 and $BiVO_4$ have an indirect and direct band gap respectively, thus the y axis of the Tauc plot is $(ah\nu^{1/2}$ for WO_3 and $(ah\nu)^2$ for $BiVO_4$. In Fig. 3B, the extrapolation of the Tauc plot on x intercepts gives optical band gaps of 2.77, 2.53 and 2.54 eV for Ti_{web} photoanodes covered by WO_3, $BiVO_4$ and WO_3/BiVO4, respectively. These values are in good agreement with the literature [15].

The surface morphology of the samples was studied using a scanning electron microscope. Except for some rare cracks, the WO_3 layers appear highly homogeneous (Fig. 2D). They show a low roughness, and seem to cover the titanium substrate efficiently. The $BiVO_4$ particles deposited by the SILAR method are measured to be around 180 nm and are well distributed on the electrode surface, providing good nanostructuring, even if few agglomerates can be observed in some regions (Fig. 2E).

3.2. Photoelectrochemical characterization

The synergistic association of WO_3 and $BiVO_4$ has already been described in the literature [2,7,16]. However, since the type of electrode support and the deposition techniques are different in our case, we initially compared the activities of each photoactive layer separately and prior to the measurement of combined layers.

As shown in Fig. 3A, relatively low currents were obtained under irradiation using the two semiconductors individually (0.10 and 0.25 $mA{\cdot}cm^{-2}$ for WO_3 and $BiVO_4$, respectively). The results obtained in the aqueous phase confirm that our fabrication process does form a synergistic $WO_3/BiVO_4$ heterojunction, since the photocurrent in this case can reach up to 2.3 $mA{\cdot}cm^{-2}$.

The crystallinity of the WO_3 photoanode is not the same as the WO_3 under-layer in the $WO_3/BiVO_4$ photoanodes (Fig. 2A) since the fabrication of $WO_3/BiVO_4$ involves consecutive annealing processes. This means that the direct comparison of WO_3 with $WO_3/BiVO_4$ photoanode is not applicable in this case. Nevertheless, as demonstrated in Fig. 3A, our main goal to improve the $BiVO_4$ performance building the $WO_3/BiVO_4$ junction has been achieved.

To reach the performance depicted in Fig. 3A, we studied the effect of the $BiVO_4$ loading onto the WO_3 layer (Fig. 3B). To achieve this, we compared the activity of the $WO_3/BiVO_4$ assemblies after successive steps of 10-SILAR-cycles from 10 up to 60 cycles.

All the samples share the same photocurrent onset (about + 0.4 V vs RHE) and exhibit a linear current increase through the scanned potentials. At the thermodynamic water oxidation potential the 10-cycle sample give the lowest photocurrent with 0.65 $mA{\cdot}cm^{-2}$ while the maximum activity, i.e. 1.9 $mA{\cdot}cm^{-2}$, is reached after 40 cycles. Further SILAR cycles lead to a current drop, and thus we consider that the electrode surface starts to get saturated after 40 SILAR-cycles.

Fig. 3C depicts the activity comparison between liquid and solid electrolyte operation (i.e. in PEM-PEC cell). The photoelectrochemical performances are almost identical in terms of photocurrent profile and intensity (1.9 $mA{\cdot}cm^{-2}$ at the thermodynamic potential) and regarding the photocatalytic current onset (+ 0.4 V vs RHE). This is several orders of magnitude higher than any other visible light activated solid state electrolyte system [3–6], confirming the strong potential of our reactor and electrode design.

The possibility of using the PEM-PEC cell to capture and use water molecules from the ambient air has been nicely demonstrated by Ronge et al. [6]. The potential of this operation mode is based on the fact that solar hydrogen can be produced from a "water-neutral" process. Therefore, we investigated the operation of our PEM-PEC cell using air and He separately as carrier gases (Fig. 3C). Molecular oxygen induces current loss through a photoelectron quenching process [3,6] however at high applied potentials the performances obtained were almost identical using the two carriers, showing the great potential of our photoelectrode design for air-based PEM-PEC applications.

In order to determine the Faradaic efficiency of our system for the splitting reaction, we performed online oxygen and hydrogen detection measurements in anodic and cathodic compartments of the PEM-PEC using a quadrupole M/S for the $WO_3/BiVO_4$ photoanode (of 40 SILAR-cycles). As shown in Fig. 3D, the PEM-PEC cell splits water at a rate of 3.4 nmol O_2/s and 7.1 nmol H_2/s (i.e. O_2/H_2 ratio equal to 0.48) at the thermodynamic potential. These values correspond to a Faradaic efficiency close to ~85%.

The stability of the 40 SILAR-cycles $WO_3/BiVO_4$ photoanode was evaluated at 1.23 V vs RHE under conventional operation (i.e. with liquid electrolyte). The photocurrent decreases with time and after 1 h of illumination there is a 10% loss of photoactivity. Addition of protective layers (e.g. TiO_2 by atomic layer deposition) and co-catalysts have been planned to improve the stability and activity of our photoanodes.

In general, the results demonstrate good compatibility between the photoanodes and the solid electrolyte PEM-PEC cell design, e.g. the porosity is high enough to maintain the activity while the substrate is exposed to the gas phase reactants.

4. Conclusions

A new method of preparing highly porous $WO_3/BiVO_4$ photoanodes was demonstrated. The photoanodes are efficient under gas phase operation and compatible with our innovative solid electrolyte photoelectrochemical setup. Using our concept, this is the first time that gas phase water splitting exhibits performances similar to those of classical liquid electrolyte photoelectrochemical cells under visible light irradiation and without the use of a co-catalyst.

Acknowledgments

This work is part of the programme 'CO_2-neutral fuels', which is financially supported by the Netherlands Organisation for Scientific Research (NWO) and Shell Global Solutions (Grant No. 700.001.516.50).

References

[1] K. Sivula, R. van de Krol, Semiconducting materials for photoelectrochemical energy conversion, Nat. Rev. Mater. 1 (2) (2016) 1510–1527.
[2] R. van de Kroel, M. Gratzel, Photoelectrochemical Hydrogen Production, Springer, New York, 2012.
[3] T. Stoll, G. Zafeiropoulos, M.N. Tsampas, Solar fuel production in a novel polymeric electrolyte membrane photoelectrochemical (PEM-PEC) cell with a web of titania nanotube arrays as photoanode and gaseous reactants, Int. J. Hydrog. Energy 41 (2016) 17807–17817.
[4] J. Georgieva, S. Armyanov, I. Poulios, S. Sotiropoulos, An all-solid photoelectrochemical cell for the photooxidation of organic vapours under ultraviolet and visible light illumination, Electrochem. Commun. 11 (2009) 1643–1646.
[5] K. Xu, A. Chatzitakis, T. Norby, Solid-state photoelectrochemical cell with TiO_2 nanotubes for water splitting, Photochem. Photobiol. Sci. 16 (2017) 10–16.
[6] J. Rongé, S. Deng, S. Pulinthanathu Sree, T. Bosserez, S.W. Verbruggen, N. Kumar Singh, J. Dendooven, M.B.J. Roeffaers, F. Taulelle, M. De Volder, C. Detavernier, J.A. Martens, Air-based photoelectrochemical cell capturing water molecules from ambient air for hydrogen production, RSC Adv. 4 (2014) 29286–29290.
[7] J. Su, L. Guo, N. Bao, C.A. Grimes, Nanostructured $WO_3/BiVO_4$ heterojunction films for efficient photoelectrochemical water splitting, Nano Lett. 11 (2011) 1928–1933.
[8] F.F. Abdi, N. Firet, R. van de Krol, Efficient $BiVO_4$ thin film photoanodes modified with cobalt phosphate catalyst and W-doping, ChemCatChem 5 (2013) 490–496.
[9] L. Chen, F.M. Toma, J.K. Cooper, A. Lyon, Y. Lin, I.D. Sharp, J.W. Ager, Mo-doped $BiVO_4$ photoanodes synthesized by reactive sputtering, ChemSusChem 8 (2015) 1066–1072.
[10] F. Amano, A. Shintani, K. Tsurui, Y.M. Hwang, Fabrication of tungsten trioxide photoanode with titanium microfibers as a three dimensional conductive back contact, Mater. Lett. 199 (2017) 68–71.
[11] Y. Li, J. Zhu, H. Zhou, J. Wei, F. Liu, M. Lv, J. Tang, B. Zhang, J. Yao, Z. Huo, L. Hu, S. Dai, $BiVO_4$ semiconductor sensitized solar cells, SCIENCE CHINA Chem. 58 (2015) 1489–1493.
[12] T.W. Kim, K.S. Choi, Nanoporous $BiVO_4$ photoanodes with dual-layer oxygen evolution catalysts for solar water splitting, Science 343 (2014) 990–994.
[13] L. Xu, M.-L. Yin, S. Liu, Agx@WO_3 core-shell nanostructure for LSP enhanced chemical sensors, Sci. Rep. 4 (2014) 6745.
[14] J. Yu, A. Kudo, Effects of structural variation on the photocatalytic performance of hydrothermally synthesized $BiVO_4$, Adv. Funct. Mater. 16 (2006) 2163–2169.
[15] S.J. Hong, S. Lee, J.S. Jang, J.S. Lee, Heterojunction $BiVO_4/WO_3$ electrodes for enhanced photoactivity of water oxidation, Energy Environ. Sci. 4 (2011) 1781–1787.
[16] L. Xia, J. Bai, J. Li, Q. Zeng, X. Li, B. Zhou, A highly efficient $BiVO_4/WO_3$/W heterojunction photoanode for visible-light responsive dual photoelectrode photocatalytic fuel cell, Appl. Catal. B Environ. 183 (2016) 224–230.